Surpassing 10% Efficiency Benchmark for Nonfullerene Organic Solar Cells by Scalable Coating in Air from Single Nonhalogenated Solvent

*Long Ye, Yuan Xiong, Qianqian Zhang, Sunsun Li, Cheng Wang, Zhang Jiang, Jianhui Hou, Wei You, and Harald Ade**

The commercialization of nonfullerene organic solar cells (OSCs) critically relies on the response under typical operating conditions (for instance, temperature and humidity) and the ability of scale-up. Despite the rapid increase in power conversion efficiency (PCE) of spin-coated devices fabricated in a protective atmosphere, the efficiencies of printed nonfullerene OSC devices by blade coating are still lower than 6%. This slow progress significantly limits the practical printing of high-performance nonfullerene OSCs. Here, a new and relatively stable nonfullerene combination is introduced by pairing the nonfluorinated acceptor IT-M with the polymeric donor FTAZ. Over 12% efficiency can be achieved in spin-coated FTAZ:IT-M devices using a single halogen-free solvent. More importantly, chlorine-free, blade coating of FTAZ:IT-M in air is able to yield a PCE of nearly 11% despite a humidity of ≈50%. X-ray scattering results reveal that large π–π coherence length, high degree of face-on orientation with respect to the substrate, and small domain spacing of ≈20 nm are closely correlated with such high device performance. The material system and approach yield the highest reported performance for nonfullerene OSC devices by a coating technique approximating scalable fabrication methods and hold great promise for the development of low-cost, low-toxicity, and high-efficiency OSCs by high-throughput production.

Nonfullerene organic semiconductors have achieved significant breakthroughs in the field of photovoltaics and transistors.[1–3] Due to intensive research efforts in chemical tailoring of nonfullerene small molecular acceptors (NFAs), NFA-based organic solar cells (OSCs) are now outperforming conventional fullerene-based OSCs and have remarkable potential as a renewable and low-cost energy technology that possesses the advantages of lightweight, flexibility, variable or controlled absorption/color, lead-free, and low energy loss.[3–12] Despite considerable advances in the last few years, up to now most progress in nonfullerene organic solar cells with power conversion efficiency (PCE) over 10% has been made by spin coating in a protective nitrogen atmosphere, which is not scalable for the mass production of solar panels. Recent studies[13–15] indicated that transitioning the high efficiency of existing top-performing OSCs from conventional spin-coated devices to devices by scalable printing methods (as illustrated in **Figure 1**a), such as blade coating (solution shearing), slot-die coating, and roll-to-roll coating, is not that straightforward due to the different processing temperatures and film formation mechanisms. It is shown that the morphologies and drying dynamics of films made by blade coating, slot-die coating, and roll-to-roll processing are almost identical,[13] while the morphological features and device optimization strategies in blade-coated devices are largely different from those in conventionally spin-coated devices. Through these studies, it became clear that precisely optimizing the morphology and device performance of nonfullerene OSCs made by blade coating in conditions similar to those during mass production (e.g., humidity and elevated temperatures) is a key

Dr. L. Ye, Y. Xiong, Prof. H. Ade
Department of Physics
Organic and Carbon Electronics Lab (ORaCEL)
North Carolina State University
Raleigh, NC 27695, USA
E-mail: hwade@ncsu.edu
Dr. Q. Zhang, Prof. W. You
Department of Chemistry
University of North Carolina at Chapel Hill
Chapel Hill, NC 27599, USA
The ORCID identification number(s) for the author(s) of this article can be found under https://doi.org/10.1002/adma.201705485.
S. Li, Prof. J. Hou
Beijing National Laboratory for Molecular Sciences
Institute of Chemistry
Chinese Academy of Sciences
Beijing 100190, P. R. China
Dr. C. Wang
Advanced Light Source
Lawrence Berkeley National Laboratory
Berkeley, CA 94720, USA
Dr. Z. Jiang
Advanced Photon Source
Argonne National Laboratory
Argonne, IL 60439, USA

DOI: 10.1002/adma.201705485

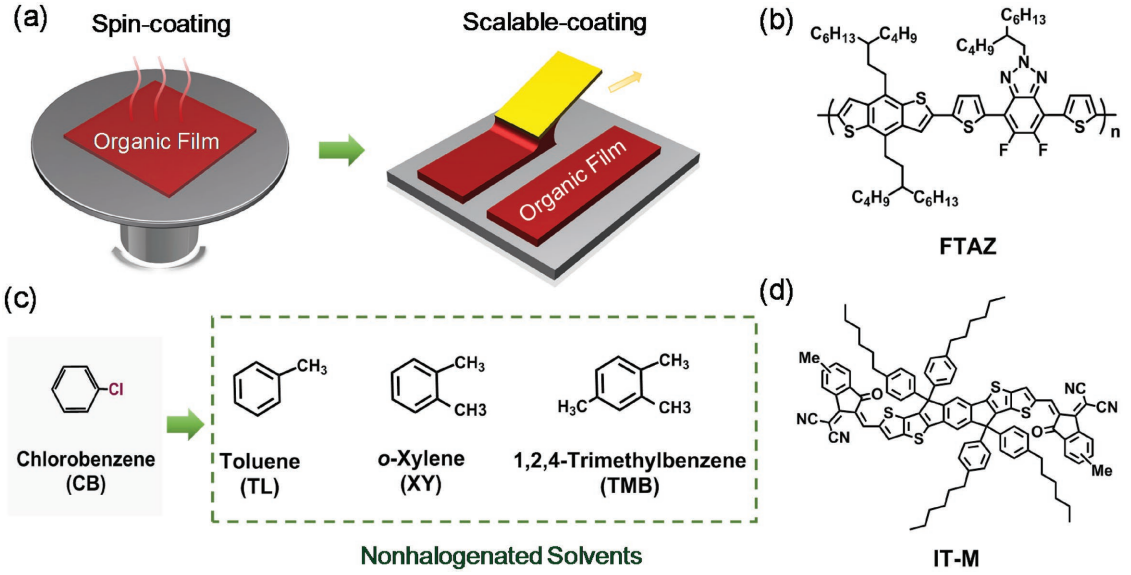

Figure 1. a) Schematic illustration of widely used spin coating and scalable coating of organic films; b) chemical structure of polymer donor FTAZ; c) chemical structures of a chlorinated solvent and several nonhalogenated solvents used in the nonfullerene OSC processing; d) chemical structure of a nonfluorinated NFA (IT-M).

step toward the ultimate commercialization of this photovoltaic technology.

Among the variety of donor polymers used in nonfullerene PSCs, the wide band-gap (≈2.0 eV) polymer donor FTAZ[16,17] (see Figure 1b) stands out as one of the best options largely due to its high hole mobility on the order of 10^{-3} cm^2 V^{-1} s^{-1} and possible morphological insensitivity.[18] In addition, FTAZ exhibits strong absorption at the wavelength range of 400–600 nm with a high absorption coefficient of 1×10^5 cm^{-1}, which is highly complementary with the absorption of many newly developed NFAs.[19,20] For example, Bauer et al.[21] paired FTAZ as the polymer donor with a perylene-based NFA, but the PCE of such blend-based devices (below 4%) was noticeably lower compared to that of FTAZ:$PC_{61}BM$ blend due to the large recombination loss. Very recently, Zhan and co-workers[20] reported an impressively high efficiency of 12.1% in spin-coated single junction OSCs from chloroform/1,8-diiodooctane by blending a new fluorinated NFA with FTAZ. Their results suggest that carefully synthesized NFAs with fluorine substituents can provide significantly higher efficiency compared with the nonfluorinated counterparts. However, these high-efficiency fluorinated NFAs usually require multiple step syntheses and thus the limited quantities/yields produced severely restrict the material accessibility and device upscaling by researchers. Another important aspect for commercialization is to realize environmentally benign fabrication of OSC devices. This requires the use of low-toxicity, halogen-free solvents. In all previous studies of FTAZ:fullerene and FTAZ:NFA blends, only chlorinated solvents such as trichlorobenzene, chloroform, and chlorobenzene (CB) were used as the processing solvent. It is generally acknowledged that these halogenated solvents are detrimental to the environment and should be avoided for printing devices,[22] in particular, in large-scale production. As such, realizing high efficiency in printed nonfullerene OSCs via scalable materials and less toxic solvents remains a grand challenge.

To address this key challenge, we report here a chlorine-free upscaling of nonfullerene OSCs (see Figure 1) based on a new photoactive polymer:NFA combination by using a single chlorine-free solvent, in the absence of solvent additives. The nonfullerene combination comprises FTAZ and a nonfluorinated NFA named IT-M (the chemical structure is shown Figure 1d),[23,24] which is now commercially available. An average efficiency up to ≈12% can be consistently achieved in spin-coated FTAZ:IT-M devices in a nitrogen atmosphere despite using a single halogen-free solvent. We are able to breach the 10% efficiency benchmark by blade coating in air with an average humidity of 50%, and the highest efficiency achieved (≈11%) is the best PCE for blade-coated OSCs to date. Furthermore, we investigate the relationship between processing solvent, drying dynamics, molecular packing, thin-film morphology, and device performance in these blade-coated films. Comparative studies of three hydrocarbon solvents (Figure 1c), namely, toluene (TL), *o*-xylene (XY), and 1,2,4-trimethylbenzene (TMB), indicate quantified morphological parameters (e.g., π–π coherence length, face-on to edge-on ratio, domain spacing and purity) correlate well to the key performance metrics of these printed devices. Our results suggest that FTAZ:IT-M is not only a model system for identifying key solvent–morphology–performance relations, but also a promising candidate for upscaling in industrial printing. Significantly, the upscaling practice shown here is expected to be widely applicable for a large class of polymer:NFA combinations, considering FTAZ and its derivatives are becoming increasingly studied in the field of nonfullerene OSCs.[4,19,20,25,26]

We started out our investigation by evaluating the basic properties of FTAZ and IT-M. **Figure 2**a shows the ultraviolet–visible (UV–vis) absorption spectra of the films of FTAZ and IT-M, suggesting a broad and complementary light-harvesting range (300-800 nm) of the FTAZ:IT-M blend (see Figure S1, Supporting Information). Also, their energy levels (Figure 2b)

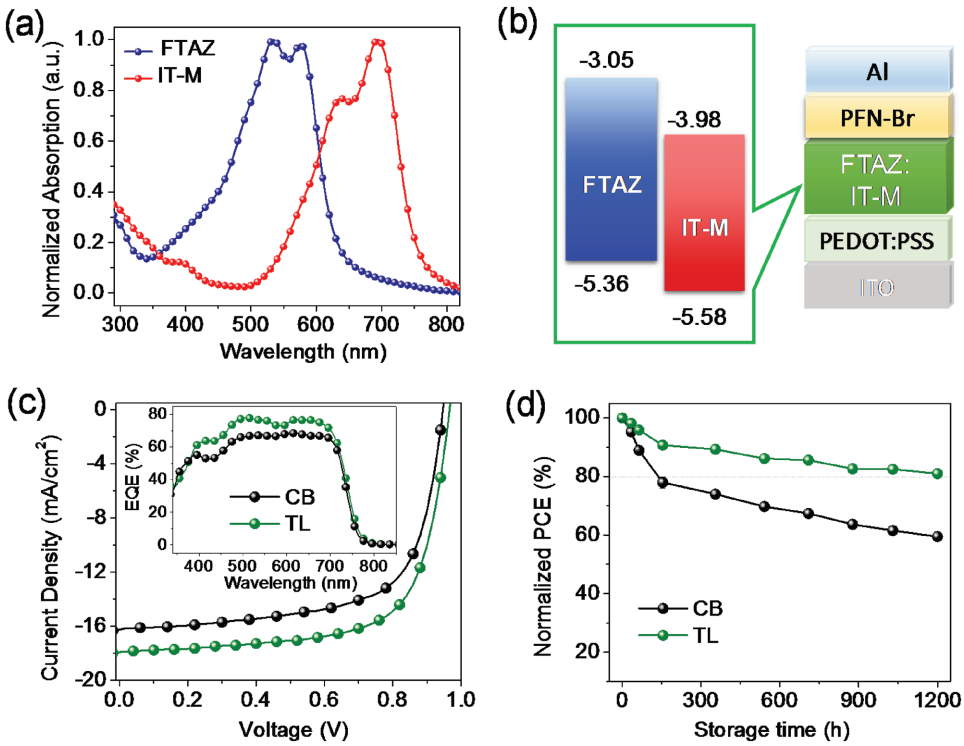

Figure 2. a) Absorption spectra of neat FTAZ and IT-M films; b) energy diagrams of FTAZ and IT-M, and device configuration used in this work; c) representative *J*–*V* curves and EQE curves of FTAZ:IT-M devices processed by CB and TL in the nitrogen atmosphere recorded under AM 1.5G 100 mW cm^{-2} irradiation; d) normalized PCEs of unencapsulated device as a function of storage time in the nitrogen under dark.

are quite matched with a sufficient energy offset for charge creation. Through simple solubility tests at room temperature, we find both FTAZ and IT-M can be well dissolved in several hydrocarbon solvents, such as toluene, *o*-xylene, and 1,2,4-trimethylbenzene. Good solubilities (>8 mg mL^{-1}) afforded by those hydrocarbon solvents allow us to make uniform FTAZ:IT-M films. To assess the potential of this new combination for OSC applications, nonfullerene OSCs with TL and CB respectively as process solvents are fabricated in a regular device architecture (Figure 2b), where PEDOT:PSS was used as a hole-transporting layer and an alcohol-soluble material PFN–Br[27] as the electron-transporting layer buffer layer to the metal cathode. After optimizing the processing parameters such as D/A weight ratio (Table S1, Supporting Information) and film thickness, 1:1 weight ratio was used to make a 105 ± 5 nm thick film. Notably, no solvent additive was needed. The spin-coated films were dried/annealed at 150 °C for 10 min. The detailed descriptions of the device fabrications are available in the Supporting Information. The current density–voltage (*J*–*V*) characteristics of the nonfullerene OSCs measured under simulated AM 1.5 G irradiation (with the intensity of 100 mW cm^{-2}) are shown in Figure 2c and the device parameters are summarized in Table S2 (Supporting Information). Using the halogen-free solvent TL, we were able to achieve an average PCE of 12.0 ± 0.1% in spin-coated devices. As a control, a lower PCE of 10.5 ± 0.3% is obtained when CB is used due to the relative lower fill-factor (FF) and short-circuit current density (J_{sc}). The external quantum efficiency (EQE) values shown in Figure 2c are in a good agreement with the observed J_{sc} from *J*–*V* tests, indicating the advantage of nonhalogenated solvents in this system. We note that the low absorption range (350–450 nm) of nonfullerene OPVs can still deliver a high EQE of ≈60%, which has been observed in other literature reports[20,25] and are mainly due to the efficient exciton dissociation and charge collection as reflected by the morphology. Unlike previous reports on FTAZ:fluorinated NFA[19,20] where fluorination was believed to play an important role, it is intriguing to note that matching FTAZ with a nonfluorinated IT-M in our case is able to yield over 12% efficiency by spin coating in the nitrogen atmosphere. This implies fluorinated NFA is not a prerequisite for achieving high-efficiency by pairing with FTAZ. We also note that the TL devices without encapsulation can maintain over 80% of the original performance after storing in the nitrogen atmosphere under the dark condition for 1200 h (Figure 2d), while the PCE of CB devices drops much faster, which might be due to the relatively poor morphological stability (e.g., larger size phase separation occurs after aging) of CB devices, as shown in a recent study.[28] These results clearly indicate that one can use greener solvents to replace the dominating chlorinated solvents currently used in fabricating nonfullerene OSCs. Overall, our new combination of FTAZ:IT-M is a promising candidate system for scalable coating due to halogen-free processing and good stability.

Inspired by these results from spin coating, we directed our attention to chlorine-free blade coating of this new system in air (**Figure 3**a). The processing was done in lab air with ≈50% relative humidity (see Figure S2 in the Supporting Information) highlighting that ability to translate to cost-effective

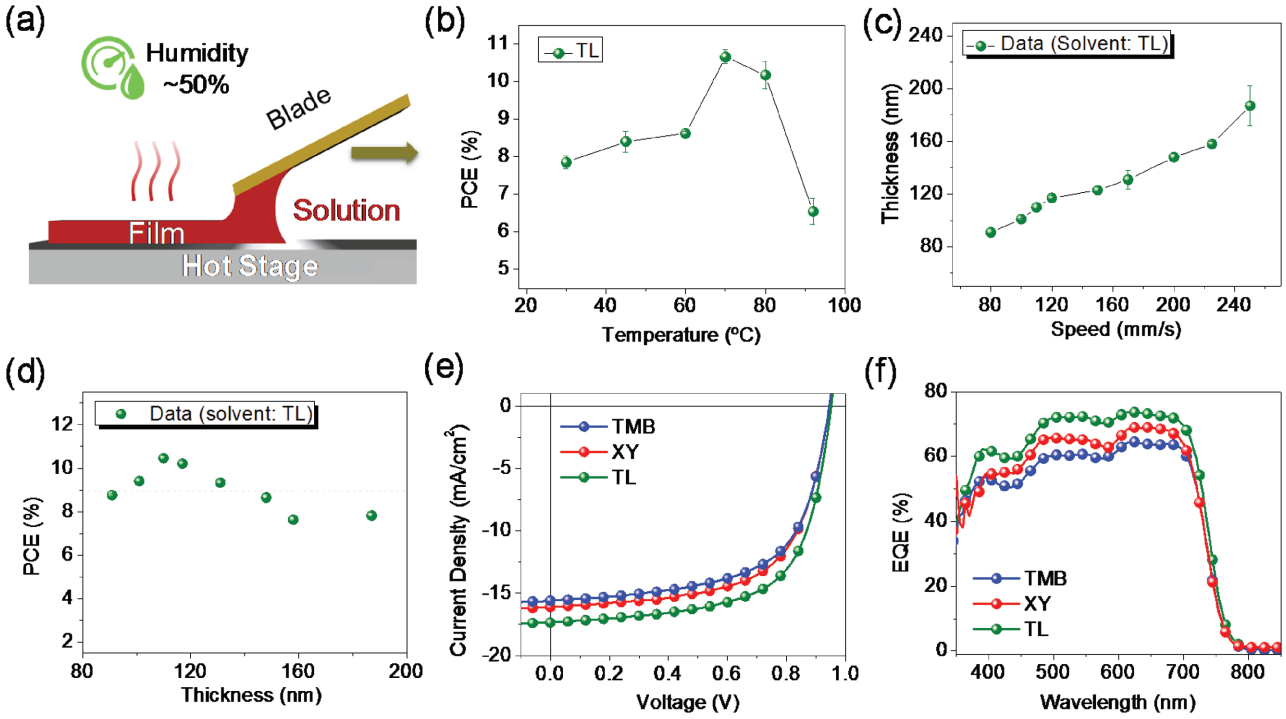

Figure 3. a) Schematic representation of the adopted scalable processing, i.e., chlorine-free blade-coating in air (having an average humidity of 50%) with a single solvent; b) device PCE of the blade-coated FTAZ:IT-M film with TL as a function of the temperature of hot stage; c) thickness of the TL-processed FTAZ:IT-M film as a function of blade speed, and the error bars of thickness are calculated from 4 spots; d) device PCE of the blade-coated FTAZ:IT-M film with TL as a function of thickness; e) representative *J*–*V* curves and f) EQE curves recorded under the illumination of AM 1.5G 100 mW cm^{-2}.

fabrication. Optimization of the conditions for blade coating of the photoactive layers is summarized in the Supporting Information. For successive optimization, a chlorine-free TL solution of FTAZ:IT-M blend was deposited using a custom-built blade coater (the schematic setup is shown in the inset of Figure 3a) and the coating temperature (i.e., the temperature of the hot stage) was screened first (Figure S3 and Table S3, Supporting Information) and the PCE of the respective devices was recorded. As shown in Figure 3b, we were able to achieve an average PCE greater than 10% when the coating temperature was 70—80 °C and the optimum performance of nearly 11% can be achieved at 70 °C, while the device FF was significantly lower when the coating temperature was below 70 °C or above 80 °C. Our data clearly suggest that the coating temperature is a critical parameter for scalable coating of the blend films, and this finding is in line with the previous reports of blade-coating polymer:fullerene OSCs.[13,14,29] Additionally, the film thickness can be readily tuned from 80 to 200 nm by altering the blade speed for a fixed solution concentration of 16 mg mL^{-1} in total. As shown in Figure 3c and Table S4 (Supporting Information), the thickness and blade speed follow a power-law relation for the speed range investigated (80–250 mm s^{-1}), which implied our deposition process is in close agreement with the Landau–Levich regime[30] due to the positive power exponent. A plot of the PCE against the thickness of TL-processed devices is displayed in Figure 3d and the corresponding *J*–*V* curves are shown in Figure S4 (Supporting Information). The device PCE is insensitive to the thickness of the active layer in the range of 90–150 nm, and ≈9% can be obtained for these thicknesses with the highest efficiency of nearly 11% appearing at a thickness of ≈110 nm.

To reveal the process–morphology–function relation in FTAZ:IT-M by this chlorine-free blade-coating, we performed a comparative investigation of the drying dynamics, photovoltaic properties, molecular packing, and phase separation of blade-coated films by using three halogen-free solvents TMB, XY, and TL. The difference of these halogen-free solvents is the number of methyls attached to the benzene ring, which varies with the boiling points and drying dynamics. Our in situ variable angle spectroscopic ellipsometry[15] experiments (see Figure S5 in the Supporting Information and additional details) suggest the drying times after the blade casting at the same temperature are 10, 6, and 2 s for TMB, XY, and TL, respectively. Correspondingly, such a distinct drying time may lead to different device performances. Using the same device architecture shown in Figure 2b, the *J*–*V* characteristics of blade-coated devices from different solvents and the associated EQE curves are shown in Figure 3e,f. As listed in **Table 1**, the open-circuit voltage (V_{oc}) is 0.94–0.95 V, irrespective of the solvent used, while the average J_{sc} is gradually increased from 14.4 to 16.8 mA cm^{-2} and the average FF from 61.9% to 66.1%, when a faster-drying solvent (TL > XY > TMB) is applied. As a result, the average and champion PCE of our blade-coated FTAZ:IT-M devices using TL are 10.6% and 11%, respectively.

To understand the performance differences of blade-coated devices resulting from three different solvents, quantification

Table 1. Photovoltaic device parameters of FTAZ:IT-M-based nonfullerene OSCs by chlorine-free blade-coating in air having an average humidity of ≈50%.

Solvent	V_{oc} [mV]	J_{sc} [mA cm^{-2}]	FF [%]	PCE[a)] [%]	Axy/Az	Domain spacing [nm]	ISI[b)]
TMB	940 ± 5	14.4 ± 0.5	61.9 ± 1.0	8.4 ± 0.3 (9.1)	1.9	32.9	0.90
XY	943 ± 5	15.7 ± 0.7	62.3 ± 1.2	9.3 ± 0.2 (9.6)	2.2	34.0	0.92
TL	950 ± 2	16.8 ± 0.3	66.1 ± 1.1	10.6 ± 0.2 (11.0)	3.1	19.9	1.00

[a)]The standard deviations of solar cell performances are averaged from ten devices and the maximum values are shown in the parentheses; [b)]Here the area of the whole lognormal peak is used as integrated scattering intensity (ISI) and this ISI is normalized to the highest value, which is set as 1. The film thickness is 105 ± 5 nm for these blade-coated samples.

of both nanoscale and mesoscale features is critical to establish a complete solvent–morphology–function relation. First, high-resolution grazing incidence wide-angle X-ray scattering (GIWAXS)[31] at Argonne National Laboratory was used to probe the molecular packing and texture of their active layers, where the volume fraction of the disordered portion is much larger than that of the ordered part.[32] As observed from the 2D GIWAXS patterns in **Figure 4**a and 1D profiles shown in Figure S6 (Supporting Information), the molecular order of blend films is gradually improved (TL > XY > TMB) when the boiling point of solvent was decreased. Particularly, we observed more pronounced (010) diffraction peak at q_z = 1.7 Å^{-1} and high orders of lamellar peaks in the in-plane (q_{xy}) direction, which reveals a preferential face-on orientation with respect to the substrate. By using the full width at half-maximum of the π–π stacking reflection peaks, we estimated the out-of-plane π–π coherence lengths of FTAZ and IT-M of these blend films via peak fitting, and both coherence lengths (Figure 4b) show the same trend: TL > XY > TMB. Here, pole figures of (100) peaks are extracted and corrected for geometry,[32,33] and a quantitative parameter A_{xy}/A_z as schematically described in Figure 4c is used for comparing the face-on to edge-on ratios across samples. We noted that the face-on to edge-on ratio is the highest (3.1) for the TL-processed devices, indicative of a more face-on tendency, while XY and TMB devices show a lower ratio of 2.2 and 1.9, respectively. It has been shown that face-on orientation enhances intermolecular charge transport and is beneficial for efficient OSCs.[33,34] Thus, the high π–π coherence length and A_{xy}/A_z are beneficial for charge transport of TL devices, which can partly explain the highest J_{sc} and FF obtained.

Resonant soft X-ray scattering (R-SoXS) was utilized to quantify the domain characteristics of these blade-coated films following detailed protocols previously established.[15,35] Figure 4d displays the Lorentz-corrected scattering profiles at a resonant X-ray energy where the scattering contrast is relatively large.

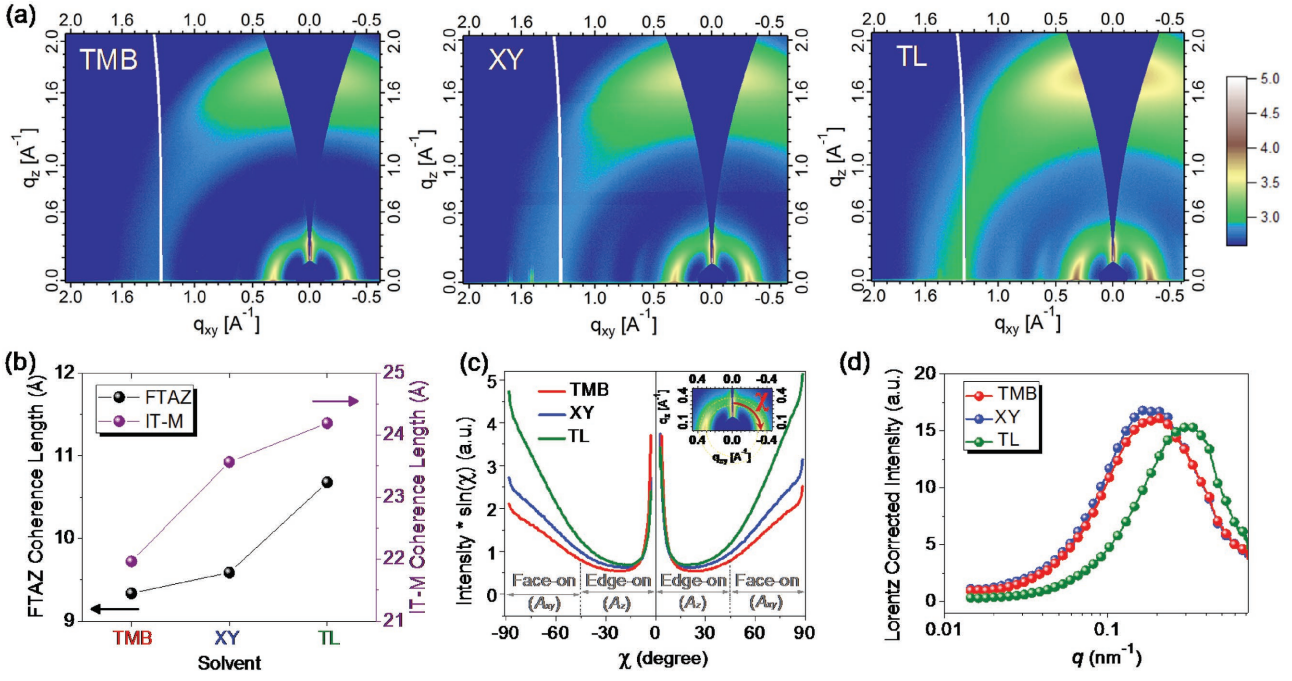

Figure 4. a) GIWAXS 2D pattern and b) out-of-plane π–π coherence lengths of FTAZ and IT-M in the blade-coated films from different solvents; c) pole figures extracted from the (100) diffraction of blade-coated FTAZ:IT-M films with TL, XY, and TMB. The inset shows the close-up of the lamellar (100) region and the definitions of the polar angle (χ) range corresponding to the edge-on (A_z) and face-on (A_{xy}) crystallites; d) Lorentz-corrected scattering profiles from azimuthally averaged R-SoXS images of blade-coated films at a photon energy of ≈284 eV.

We note that all R-SoXS profiles are dominated by a single lognormal function, similar to prior polymer:fullerene studies using FTAZ.[18] Under an assumption of globally 3D isotropic morphology, 2π over q of the dominant peak gives the center-to-center domain spacing of a given system, and the integration of the R-SoXS profile (the whole lognormal peak), i.e., integrated scattering intensity (ISI), represents the mean-square variance of the composition, which can be used to quantify the average domain purity. The details of this procedure and its justification have been documented in some recent reports.[36] The quantified parameters from R-SoXS tests are listed in Table 1, and the ISI of TMB and XY devices is respectively 90% and 92% of that of the TL device. It is shown that high domain purity is often desirable for suppressing bimolecular recombination and increase device FF.[36] Therefore, the relative domain purity as reflected by ISI here also positively correlates with the device FF. In addition, domain spacing is strongly affected by the type of solvent. The XY film shows the largest domain spacing of 34 nm and the spacing of the TMB film is very similar. In stark contrast to the XY and TMB cases, the domains of the TL film has the smallest spacing (19.9 nm), which is very close to the typical exciton diffusion length.[37] As small domains close to this length are considered necessary to provide large enough D/A interfacial area, exciton dissociation and charge creation will be facilitated.[36] On the basis of the above results, a halogen-free solvent with lower boiling point enables increased face-on orientation, larger coherence lengths, and smaller domains. We conclude that halogen-free blade coating in air with TL is able to achieve the most face-on ordering and smallest domain spacing, thereby affording nearly 11% efficiency in devices.

The above findings motivated us to further understand the stability of the printed FTAZ:IT-M devices using TL. After a storage time of ≈1000 h in a glovebox, blade-coated devices using TL can attain ≈85% of the initial PCE (**Figure 5**a; Table S5, Supporting Information). Utilizing an aged FTAZ:IT-M solution in air after storing in dark for 20 days, we can still get ≈91% of the efficiency achieved from a freshly prepared solution (see Figure 5b and Table S6 in the Supporting Information, and experimental details are shown in the Supporting Information). We completed blade-coated devices after heating the active layers at 150 °C for different time periods from 10 to 240 min (Figure 5c), and the PCE can still maintain over 10% after being heated at 150 °C for 240 min. Under such a high annealing temperature, the devices J_{sc} and V_{oc} are independent of the annealing time (see Table S7 in the Supporting Information), resulting in a largely unchanged PCE (10–11%). We further fabricated a larger-area (0.56 cm^2) FTAZ:IT-M device (Figure 5d) using the same halogen-free blade-coating in air approach. The device efficiency is 9.8%, and the slightly decreased PCE and V_{oc} (Table S8 in the Supporting Information) are mainly due to the resistance loss of the top electrodes utilized (see the inset of Figure 5d). To make a comparison with the results shown in the literature, we carried out a survey (see **Table 2**) of state-of-the-art nonfullerene OSCs to date[14,15,38,39]

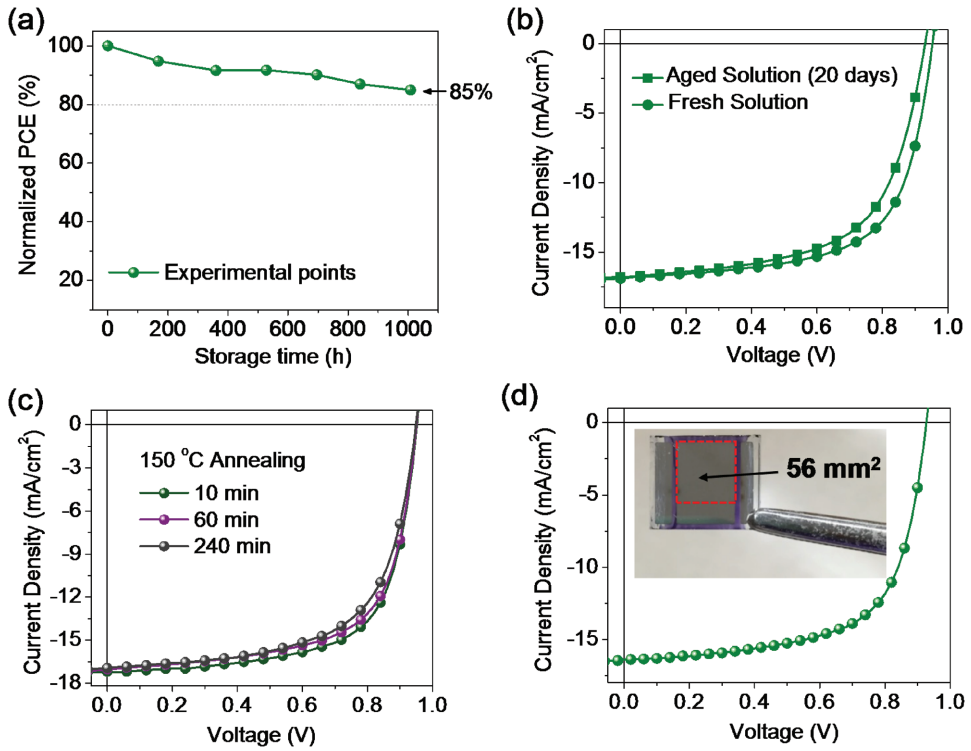

Figure 5. a) Storage stability of FTAZ:IT-M devices by halogen-free blade coating in air (average humidity: ≈50%). TL was used as the solvent. Devices were unencapsulated and stored in a glovebox; b) *J–V* characteristics of FTAZ:IT-M devices by halogen-free blade coating in air using freshly prepared solution and solution aged at room temperature for 20 d; c) *J–V* characteristics of blade-coated FTAZ:IT-M devices with active layers annealed at 150 °C for different time periods; d) *J–V* characteristics of FTAZ:IT-M devices with a larger area (0.56 cm^2). The inset is the photograph of the device and effective area.

Table 2. A survey of photovoltaic parameters and processing conditions of the state-of-the-art nonfullerene OSCs by blade-coating techniques.

Nonfullerene system	Atmosphere	Solvent[a)]	Halogen free	Device area[b)] [mm^2]	PCE_{max} [%]	Ref.
PBDT-TS1:PPDIODT	Air	*o*-MA	Yes	6.9	5.6	[15]
PBDT-TS1:PPDIODT	Air	*o*-MA	Yes	13.0	5.1	[15]
PiI-tT-PS5:P(TP)	Air	CB	No	4.0	3.2	[38]
PTB7-Th:tPDI-Hex	Air	2Me-THF	Yes	4.0	4.8	[39]
FTAZ:IT-M	Air	TL	Yes	6.9	11.0	This work
FTAZ:IT-M	Air	TL	Yes	56.0	9.8	This work

[a)]*o*-MA is *o*-metylanisole, and 2Me-THF represents 2-methyltetrahydrofuran; [b)]Effective device area.

by blade-coating techniques. The highest value shown in the literature is below 6% after taking into account all critical factors such as effective device area, solvent, and atmosphere. As a consequence, the PCE of our blade-coated nonfullerene OSC is substantially higher, by ≈90%, than that of the best blade-coated nonfullerene device reported in the literature.[15] Lastly, it is worth pointing out that more than 10 derivatives of FTAZ (the chemical structures are shown in Figure S7 in the Supporting Information) have been recently applied to spin-coated nonfullerene OSC devices. As most of these derivatives have an identical backbone (all of them are consisting of benzodithiophene and fluorinated benzotriazole) and presumably comparable solubility in nonchlorinated solvents to that of FTAZ, our method should be applicable to the morphology optimization of blade-coated devices based on these structurally similar FTAZ derivatives. Similarly, our chlorine-free blade-coating approach can be applied to other emerging NFA systems of interest, such as ITCC[40] and EH-IDTBR.[9,28,41] We note that the FF values of our new FTAZ:IT-M system are relatively low (<70%) compared with some reported high-efficiency nonfullerene OSC systems,[12,20] and the FF of FTAZ:IT-M devices might be limited by the intrinsic polymer:acceptor miscibility[24] that will depend on the donor polymer and the molecular acceptor. Further molecular engineering the chemical structures is anticipated to reduce the FF and efficiency loss.

In summary, we report spin-coated and printed OSCs of high efficiency using a new nonfullerene polymer:small molecule blend (FTAZ:IT-M) and an additive-free and halogen-free solvent processing. Our results suggest fluorinated NFAs are not necessarily required for high-performance nonfullerene OSCs, and a nonfluorinated NFA (IT-M) that is now commercially available is capable of yielding a comparable PCE with those of the state-of-the-art fluorinated NFAs when pairing with FTAZ. By blade coating with chlorine-free solvents in air, FTAZ:IT-M OSCs yields a PCE of up to 11%, which outperforms any reported nonfullerene and fullerene devices to date by blade coating. Comparative studies suggest the choice of nonchlorinated solvents not only alters the face-on orientation, but also significantly affects the domain purities and length scales of phase separation of the blade-coated nonfullerene OSCs. Among the halogen-free solvents studied, toluene with the lowest boiling point is the best processing solvent for this new FTAZ:IT-M combination due to the more preferable molecular ordering and optimized domain characteristics. Furthermore, we discovered that the FTAZ:IT-M film blade-coated from TL is stable against high-temperature (150 °C) heating and its aged solution up to 20 days in air shows only a very small performance loss. Both aspects should bode well for translation into an industrial setting and for morphological stability. Together, our results represent important progress for printed nonfullerene OSCs and underscore that FTAZ:IT-M is a viable candidate for use in highly efficient and stable photovoltaic cells. Further engineering the morphology and interface characteristics of this blend system is underway.

Experimental Section

For GIWAXS characterizations, samples are placed in vacuum at beamline 8-ID-E[31] of the Advanced Photon Source, Argonne National Laboratory. The energy of the hard X-ray beam is ≈11 keV. GIWAXS data were collected with a 2D area detector (Pilatus 1M). The sample to detector distance was ≈228 mm, and the bulk was probed using an incident angle of 0.16° (i.e., above the polymer critical angle). R-SoXS[35] and reference spectrum[42] measurements were performed at beamline 11.0.1.2 and 5.3.2 at Advanced Light Source, Lawrence Berkeley National Laboratory. R-SoXS images were collected in vacuum on a 2D charge-coupled device cooled to −45 °C (Princeton Instrument PI-MTE). For the chlorine-free blade coating, a new blade-coater is used and the design is similar to our previously used blade coater[14] except that this new blade coater is more compact (see Figure S8 and details in the Supporting Information). Other experimental details can be found in the Supporting Information.

Supporting Information

Supporting Information is available from the Wiley Online Library or from the author.

Acknowledgements

L.Y. and Y.X. contributed equally to this work. This research was carried out at NCSU with supports from UNC-GA Research Opportunity Initiative grant and the NSF INFEWS grant CBET 1639429. Q.Z. and W.Y. were supported by the NSF (CBET-1639429, DMR-1507249). J. Hou gratefully acknowledges the financial support from National Nature Science Foundation of China (Grant Nos. 91633301, 91333204 and 21325419), and the Chinese Academy of Science (Grant No. XDB12030200). Beamlines 5.3.2.2 and 11.0.1.2 at the Advanced Light Source are supported by the Director of the Office of Science, Office of Basic Energy Sciences, of the U.S. Department of Energy under Contract No. DE-AC02-05CH11231. Use of the Advanced Photon Source was

supported by the U.S. Department of Energy, Office of Science, Office of Basic Energy Sciences, under Contract DE-AC02-06CH11357. We gratefully acknowledge the beamline support at beamlines 5.3.2.2 and 11.0.1.2 provided by C. Wang, Y. Yu, and A.L.D. Kilcoyne. Prof. Brendan O'Connor and Nrup Balar are acknowledged for the discussion and help with the in situ ellipsometry data analysis. We appreciate Dr. Abay Dinku for maintaining and operating the shared device fabrication facilities.

Conflict of Interest

The authors declare no conflict of interest.

Keywords

blade coating, film morphology, nonfullerene acceptors, nonhalogenated solvents, organic solar cells

Received: September 21, 2017
Revised: November 2, 2017
Published online: January 10, 2018

[1] A. F. Paterson, N. D. Treat, W. Zhang, Z. Fei, G. Wyatt-Moon, H. Faber, G. Vourlias, P. A. Patsalas, O. Solomeshch, N. Tessler, M. Heeney, T. D. Anthopoulos, *Adv. Mater.* **2016**, *28*, 7791.
[2] Y. Lin, J. Wang, Z.-G. Zhang, H. Bai, Y. Li, D. Zhu, X. Zhan, *Adv. Mater.* **2015**, *27*, 1170.
[3] J. Liu, S. Chen, D. Qian, B. Gautam, G. Yang, J. Zhao, J. Bergqvist, F. Zhang, W. Ma, H. Ade, O. Inganäs, K. Gundogdu, F. Gao, H. Yan, *Nat. Energy* **2016**, *1*, 16089.
[4] H. Bin, L. Gao, Z.-G. Zhang, Y. Yang, Y. Zhang, C. Zhang, S. Chen, L. Xue, C. Yang, M. Xiao, Y. Li, *Nat. Commun.* **2016**, *7*, 13651.
[5] Y. Lin, X. Zhan, *Mater. Horiz.* **2014**, *1*, 470.
[6] a) Y. Liu, Z. Zhang, S. Feng, M. Li, L. Wu, R. Hou, X. Xu, X. Chen, Z. Bo, *J. Am. Chem. Soc.* **2017**, *139*, 3356; b) F. Liu, Z. Zhou, C. Zhang, J. Zhang, Q. Hu, T. Vergote, F. Liu, T. P. Russell, X. Zhu, *Adv. Mater.* **2017**, *29*, 1606574; c) B. Guo, W. Li, X. Guo, X. Meng, W. Ma, M. Zhang, Y. Li, *Adv. Mater.* **2017**, *29*, 1702291.
[7] D. M. Stoltzfus, J. E. Donaghey, A. Armin, P. E. Shaw, P. L. Burn, P. Meredith, *Chem. Rev.* **2016**, *116*, 12920.
[8] C. B. Nielsen, S. Holliday, H.-Y. Chen, S. J. Cryer, I. McCulloch, *Acc. Chem. Res.* **2015**, *48*, 2803.
[9] S. Chen, Y. Liu, L. Zhang, P. C. Y. Chow, Z. Wang, G. Zhang, W. Ma, H. Yan, *J. Am. Chem. Soc.* **2017**, *139*, 6298.
[10] D. Baran, R. S. Ashraf, D. A. Hanifi, M. Abdelsamie, N. Gasparini, J. A. Rohr, S. Holliday, A. Wadsworth, S. Lockett, M. Neophytou, C. J. Emmott, J. Nelson, C. J. Brabec, A. Amassian, A. Salleo, T. Kirchartz, J. R. Durrant, I. McCulloch, *Nat. Mater.* **2017**, *16*, 363.
[11] Y. Zhong, M. T. Trinh, R. Chen, G. E. Purdum, P. P. Khlyabich, M. Sezen, S. Oh, H. Zhu, B. Fowler, B. Zhang, W. Wang, C. Y. Nam, M. Y. Sfeir, C. T. Black, M. L. Steigerwald, Y. L. Loo, F. Ng, X. Y. Zhu, C. Nuckolls, *Nat. Commun.* **2015**, *6*, 8242.
[12] W. Zhao, S. Li, H. Yao, S. Zhang, Y. Zhang, B. Yang, J. Hou, *J. Am. Chem. Soc.* **2017**, *139*, 7148.
[13] H. W. Ro, J. M. Downing, S. Engmann, A. A. Herzing, D. M. DeLongchamp, L. J. Richter, S. Mukherjee, H. Ade, M. Abdelsamie, L. K. Jagadamma, A. Amassian, Y. Liu, H. Yan, *Energy Environ. Sci.* **2016**, *9*, 2835.
[14] L. Ye, Y. Xiong, H. Yao, A. Gadisa, H. Zhang, S. Li, M. Ghasemi, N. Balar, A. Hunt, B. T. O'Connor, J. Hou, H. Ade, *Chem. Mater.* **2016**, *28*, 7451.
[15] a) L. Ye, Y. Xiong, S. Li, M. Ghasemi, N. Balar, J. Turner, A. Gadisa, J. Hou, B. T. O'Connor, H. Ade, *Adv. Funct. Mater.* **2017**, *27*, 1702016; b) S. Mukherjee, A. A. Herzing, D. L. Zhao, Q. H. Wu, L. P. Yu, H. Ade, D. M. DeLongchamp, L. J. Richter, *J. Mater. Res.* **2017**, *32*, 1921.
[16] S. C. Price, A. C. Stuart, L. Yang, H. Zhou, W. You, *J. Am. Chem. Soc.* **2011**, *133*, 4625.
[17] W. Li, S. Albrecht, L. Yang, S. Roland, J. R. Tumbleston, T. McAfee, L. Yan, M. A. Kelly, H. Ade, D. Neher, W. You, *J. Am. Chem. Soc.* **2014**, *136*, 15566.
[18] J. R. Tumbleston, A. C. Stuart, E. Gann, W. You, H. Ade, *Adv. Funct. Mater.* **2013**, *23*, 3463.
[19] S. Dai, F. Zhao, Q. Zhang, T.-K. Lau, T. Li, K. Liu, Q. Ling, C. Wang, X. Lu, W. You, X. Zhan, *J. Am. Chem. Soc.* **2017**, *139*, 1336.
[20] F. Zhao, S. Dai, Y. Wu, Q. Zhang, J. Wang, L. Jiang, Q. Ling, Z. Wei, W. Ma, W. You, C. Wang, X. Zhan, *Adv. Mater.* **2017**, *29*, 1700144.
[21] N. Bauer, Q. Zhang, J. Zhao, L. Ye, J.-H. Kim, I. Constantinou, L. Yan, F. So, H. Ade, H. Yan, W. You, *J. Mater. Chem. A* **2017**, *5*, 4886.
[22] J. Zhao, Y. Li, G. Yang, K. Jiang, H. Lin, H. Ade, W. Ma, H. Yan, *Nat. Energy* **2016**, *1*, 15027.
[23] S. Li, L. Ye, W. Zhao, S. Zhang, S. Mukherjee, H. Ade, J. Hou, *Adv. Mater.* **2016**, *28*, 9423.
[24] L. Ye, W. Zhao, S. Li, S. Mukherjee, J. H. Carpenter, O. Awartani, X. Jiao, J. Hou, H. Ade, *Adv. Energy Mater.* **2017**, *7*, 1602000.
[25] J. Wang, W. Wang, X. Wang, Y. Wu, Q. Zhang, C. Yan, W. Ma, W. You, X. Zhan, *Adv. Mater.* **2017**, *29*, 1702125.
[26] L. Xue, Y. Yang, J. Xu, C. Zhang, H. Bin, Z. G. Zhang, B. Qiu, X. Li, C. Sun, L. Gao, J. Yao, X. Chen, Y. Yang, M. Xiao, Y. Li, *Adv. Mater.* **2017**, *29*, 1703344.
[27] B. Fan, K. Zhang, X.-F. Jiang, L. Ying, F. Huang, Y. Cao, *Adv. Mater.* **2017**, *29*, 1606396.
[28] A. Wadsworth, R. S. Ashraf, M. Abdelsamie, S. Pont, M. Little, M. Moser, Z. Hamid, M. Neophytou, W. M. Zhang, A. Amassian, J. R. Durrant, D. Baran, I. McCulloch, *ACS Energy Lett.* **2017**, *2*, 1494.
[29] K. L. Gu, Y. Zhou, X. Gu, H. Yan, Y. Diao, T. Kurosawa, B. Gan apathysubramanian, M. F. Toney, Z. Bao, *Org. Electron.* **2017**, *40*, 79.
[30] M. Le Berre, Y. Chen, D. Baigl, *Langmuir* **2009**, *25*, 2554.
[31] Z. Jiang, X. F. Li, J. Strzalka, M. Sprung, T. Sun, A. R. Sandy, S. Narayanan, D. R. Lee, J. Wang, *J. Synchrotron Radiat.* **2012**, *19*, 627.
[32] J. Rivnay, S. C. B. Mannsfeld, C. E. Miller, A. Salleo, M. F. Toney, *Chem. Rev.* **2012**, *112*, 5488.
[33] V. Vohra, K. Kawashima, T. Kakara, T. Koganezawa, I. Osaka, K. Takimiya, H. Murata, *Nat. Photonics* **2015**, *9*, 403.
[34] a) P. M. Beaujuge, J. M. J. Fréchet, *J. Am. Chem. Soc.* **2011**, *133*, 20009; b) Q. Zhang, B. Kan, F. Liu, G. K. Long, X. J. Wan, X. Q. Chen, Y. Zuo, W. Ni, H. J. Zhang, M. M. Li, Z. C. Hu, F. Huang, Y. Cao, Z. Q. Liang, M. T. Zhang, T. P. Russell, Y. S. Chen, *Nat. Photonics* **2015**, *9*, 35.
[35] a) E. Gann, A. T. Young, B. A. Collins, H. Yan, J. Nasiatka, H. A. Padmore, H. Ade, A. Hexemer, C. Wang, *Rev. Sci. Instrum.* **2012**, *83*, 045110; b) F. Liu, M. A. Brady, C. Wang, *Eur. Polym. J.* **2016**, *81*, 555.
[36] a) J. H. Carpenter, A. Hunt, H. Ade, *J. Electron Spectrosc. Relat. Phenom.* **2015**, *200*, 2; b) X. Jiao, L. Ye, H. Ade, *Adv. Energy Mater.* **2017**, *7*, 1700084.
[37] F. Liu, Y. Gu, J. W. Jung, W. H. Jo, T. P. Russell, *J. Polym. Sci., Part B: Polym. Phys.* **2012**, *50*, 1018.

[38] Y. Diao, Y. Zhou, T. Kurosawa, L. Shaw, C. Wang, S. Park, Y. Guo, J. A. Reinspach, K. Gu, X. Gu, B. C. K. Tee, C. Pang, H. Yan, D. Zhao, M. F. Toney, S. C. B. Mannsfeld, Z. Bao, *Nat. Commun.* **2015**, *6*, 7955.
[39] S. V. Dayneko, A. D. Hendsbee, G. C. Welch, *Chem. Commun.* **2017**, *53*, 1164.
[40] H. Yao, L. Ye, J. Hou, B. Jang, G. Han, Y. Cui, G. M. Su, C. Wang, B. Gao, R. Yu, H. Zhang, Y. Yi, H. Y. Woo, H. Ade, J. Hou, *Adv. Mater.* **2017**, *29*, 1700254.
[41] S. Holliday, R. S. Ashraf, A. Wadsworth, D. Baran, S. A. Yousaf, C. B. Nielsen, C.-H. Tan, S. D. Dimitrov, Z. Shang, N. Gasparini, M. Alamoudi, F. Laquai, C. J. Brabec, A. Salleo, J. R. Durrant, I. McCulloch, *Nat. Commun.* **2016**, *7*, 11585.
[42] A. L. D. Kilcoyne, T. Tyliszczak, W. F. Steele, S. Fakra, P. Hitchcock, K. Franck, E. Anderson, B. Harteneck, E. G. Rightor, G. E. Mitchell, A. P. Hitchcock, L. Yang, T. Warwick, H. Ade, *J. Synchrotron Radiat.* **2003**, *10*, 125.